

Asymptotic kinematics of Globular Clusters: the emergence of a Tully-Fisher relation.

X. Hernandez, A. J. Lara-D.I.

Instituto de Astronomía, Universidad Nacional Autónoma de México, Apartado Postal 70–264 C.P. 04510 México D.F. México.

Released 11/09/2019

ABSTRACT

Using a recent homogeneous sample of 40 high quality velocity dispersion profiles for Galactic globular clusters, we study the low gravitational acceleration regime relevant to the outskirts of these systems. We find that a simple empirical profile having a central Gaussian component and a constant large radius asymptote, σ_∞ , accurately describes the variety of observed velocity dispersion profiles. We use published population synthesis models, carefully tailored to each individual cluster, to estimate mass to light ratios from which total stellar masses, M , are inferred. We obtain a clear scaling, reminiscent of the galactic Tully-Fisher relation of $\sigma_\infty (kms^{-1}) = 0.084^{+0.075}_{-0.040} (M/M_\odot)^{0.3 \pm 0.051}$, which is interesting to compare to the deep MOND limit of $\sigma_\infty (kms^{-1}) = 0.2 (M/M_\odot)^{0.25}$. Under a Newtonian interpretation, our results constitute a further restriction on models where initial conditions are crafted to yield the outer flattening observed today. Within a modified gravity scheme, as the globular clusters studied are not isolated objects in the deep MOND regime, the results obtained point towards a modified gravity where the external field effect of MOND does not appear, or is much suppressed.

Key words: gravitation — stars: kinematics and dynamics — (Galaxy:)globular clusters: general

1 INTRODUCTION

A topic of current debate is whether the well established gravitational anomalies evident in the rotation curves of spiral galaxies, are due to the presence of dominant halos of as yet undetected dark matter, or perhaps indicative of a change in gravitational physics appearing in the low acceleration regime. It has been shown that these anomalies become conspicuous at acceleration scales below $a_0 = 1.2 \times 10^{-10} ms^{-1}$ (e.g. Famaey & McGaugh 2012, Lelli et al. 2017), where a_0 is the critical acceleration of MOND, Milgrom (1983). The central feature of MOND and related modified theories of gravity constructed so as not to require the hypothesis of dark matter, are for centrifugal equilibrium velocities about a baryonic mass M , which become flat at a value of $V_{TF} = (GMa_0)^{1/4}$ for large radii. The corresponding expectation for the velocity dispersion velocities of isothermal pressure supported systems is $\sigma_{TF} = 3^{-1/2} (GMa_0)^{1/4}$, e.g. McGaugh & Wolf(2010).

Globular clusters (henceforth GCs) offer an interesting independent test of the generality of the situation encountered in rotation curves of spiral galaxies, as they are

pressure supported systems where under standard cosmology no significant dark mater presence is expected, and towards their outskirts, reach the low acceleration regime of $a < a_0$. Starting with the work of Scarpa et al. (2003) and Scarpa et al. (2007), it has become apparent that beyond the $a < a_0$ threshold, the observed projected velocity dispersion profiles of Galactic globular clusters, are consistent with tending towards a finite value, as has been confirmed by e.g. the analysis of the Lane et al. (2009), Lane et al. (2010), Lane et al. (2011) data of Hernandez et al. (2013), and Sollima et al. (2016), $\sigma_{R \rightarrow \infty} = \sigma_\infty$.

This has been interpreted as evidence in favour of a modified gravity regime appearing in the $a < a_0$ regime by e.g. Hernandez et al. (2013) and Hernandez et al. (2017), but explained under a Newtonian scenario through selecting initial conditions in terms of density profiles, binary fractions and distributions and initial stellar mass functions for dynamical models, which evolve into the situation observed today. Examples of the latter case include Claydon et al. (2017) who consider the contribution of unbound stars to the resulting present day velocity dispersion profiles, obtaining an outer flattening consistent with observations, as was

also found by Kennedy (2014) by considering chaotic internal dynamics resulting from the interaction with the overall galactic potential, an effect which naturally increases with decreasing GC mass.

As an independent line of enquiry, one can go from requiring a flattening of the present day velocity dispersion profile, to exploring the mass scaling of σ_∞ , and compare to the expectations under Newtonian or modified gravity. In Hernandez et al. (2013) some of us used available HST velocity dispersion profiles for 8 GCs, and found a $\sigma_\infty \propto M^{0.31 \pm 0.06}$ scaling, for masses inferred from stellar population synthesis models by McLaughlin & van der Marel (2005), not including any dynamical assumptions.

In this letter we take advantage of the availability of the GC velocity dispersion profile catalogue of Baumgardt et al. (2019), which includes uniformly reduced high quality ground based ESO and Keck spectra from Baumgardt & Hilker (2018), as well as Gaia DR2 results, to construct the most recent and complete GC velocity dispersion profile library available. We also use stellar population modelling carefully tailored to the specific metallicities and ages of each GC treated from McLaughlin & van der Marel (2005) to obtain mass to light ratios and masses, to determine the empirical scaling of σ_∞ and M . For a sample of 40 GCs with velocity dispersion profiles having a large radial coverage allowing accurate σ_∞ inferences, we obtain $\sigma_\infty (km s^{-1}) = 0.084_{-0.040}^{+0.075} (M/M_\odot)^{0.3 \pm 0.051}$.

This letter is organised as follows: section 2 details the sample selection and velocity dispersion profile fitting, where we also compare the fitted profiles to the observed velocity dispersion observations. In section 3 we discuss the resulting σ_∞ vs. M scalings obtained, showing an equivalent globular cluster Tully-Fisher relation, and section 4 states our conclusions.

2 SAMPLE SELECTION AND VELOCITY DISPERSION PROFILE MODELLING

That it only recently became apparent that classical Newtonian King models are insufficient to describe extended velocity dispersion profiles of GC, is equivalent to the fact that the readily accessible to observation, central velocity dispersion values of these systems, are perfectly consistent with Newtonian expectations. Indeed, observed GC velocity dispersion profiles are characterised by a relatively constant central region, followed by a gradual drop, in consistency with expectations for isolated, equilibrium Newtonian systems, which however, are followed by a convergence to a finite asymptotic value. These profiles can be accurately described by the empirical profile:

$$\sigma(R) = \sigma_1 e^{-(R/R_\sigma)^2} + \sigma_\infty \quad (1)$$

The above profile was introduced in Hernandez et al. (2012), where it was shown to provide an accurate description to the empirical velocity dispersion profiles of a small sample of 8 Galactic globular clusters. Indeed, in Durazo et al. (2017) and Durazo et al. (2018), the same empirical profile was applied to pressure supported systems at scales orders of magnitude larger than those of GCs; the velocity dispersion profiles of over 300 low rotation elliptical galaxies

from the CALIFA and MANGA samples, carefully traced by the proposed empirical equation. It is through fits to equation (1) that we will characterise the velocity dispersion profiles of the GCs sample used.

As there are 3 free parameters in equation (1), we need at least three radial points in any profile to be fitted. So as to guarantee accurate fits, we consider only GCs with profiles including at least four radial points. This cut reduces the Baumgardt et al. (2019) catalogue to 69 of the 139 GCs reported. Still, large error bars in profiles having only 4, 5 or 6 points, yield fits with very large confidence intervals on the three parameters sought. In the interest of constructing a high quality sample, we exclude profiles where the relative error on any of the fitted parameters is larger than 0.6. This high quality cut removes a further 29 GCs, leaving us with our final sample of 40 objects.

After taking distances to the systems studied consistently from Baumgardt et al. (2019), table 1 gives the fitted parameters of equation (1) for the 40 GCs profiles in our final sample, together with their corresponding confidence intervals. In Figure (1) we show a selection of velocity dispersion fits from the final sample. The left column gives, from top to bottom, the GC with the largest central value, the one with the largest fractional difference between central and asymptotic value, the one with the largest asymptotic value¹ and the profile with the most points². The left column of this figure shows the clusters with the corresponding minimum values in our sample.

Thus, the eight systems shown in Figure (1) fairly cover the range of cases encountered. As can be seen from the figure, the empirical profile being fitted provides an accurate description across the various parameters of the sample, with the small caveat of a slight central overshooting appearing in a few of the high central velocity dispersion cases. This last however, does not in any way affect the accuracy with which σ_∞ is inferred, which is the parameter we are interested in here. Solid triangles and empty circles show observations from ESO Keck radial velocity spectra and Gaia DR2 data, respectively. As there is no systematic difference between the above two, we treat both data samples indistinctly throughout as comprising single profiles for each GC. Figures showing the corresponding profile fits for the entire sample, appear in the online material.

Finally, to estimate the total stellar masses of the GCs in question, we turn to the detailed population synthesis models of McLaughlin & van der Marel (2005), where independent metallicity estimates and careful HR diagram comparisons are used to infer the mass to light ratios in the V band for a very complete selection of Galactic GCs, fortunately including all the ones treated here. In the above study the main uncertainty in the resulting mass to light ratios comes from the assumed stellar mass functions. To account for this, we take as confidence intervals on the mass to light ratios of the GCs treated, the extremes of the three models provided (excluding Salpeter mass functions, see below),

¹ NGC 5139 is the second ranked in this category, but appears here so as not to repeat NGC 6441, which is the first ranked in both the first and third categories.

² NGC 104 is the second ranked in this category, but appears here so as not to repeat NGC 5139, which already appears in the figure

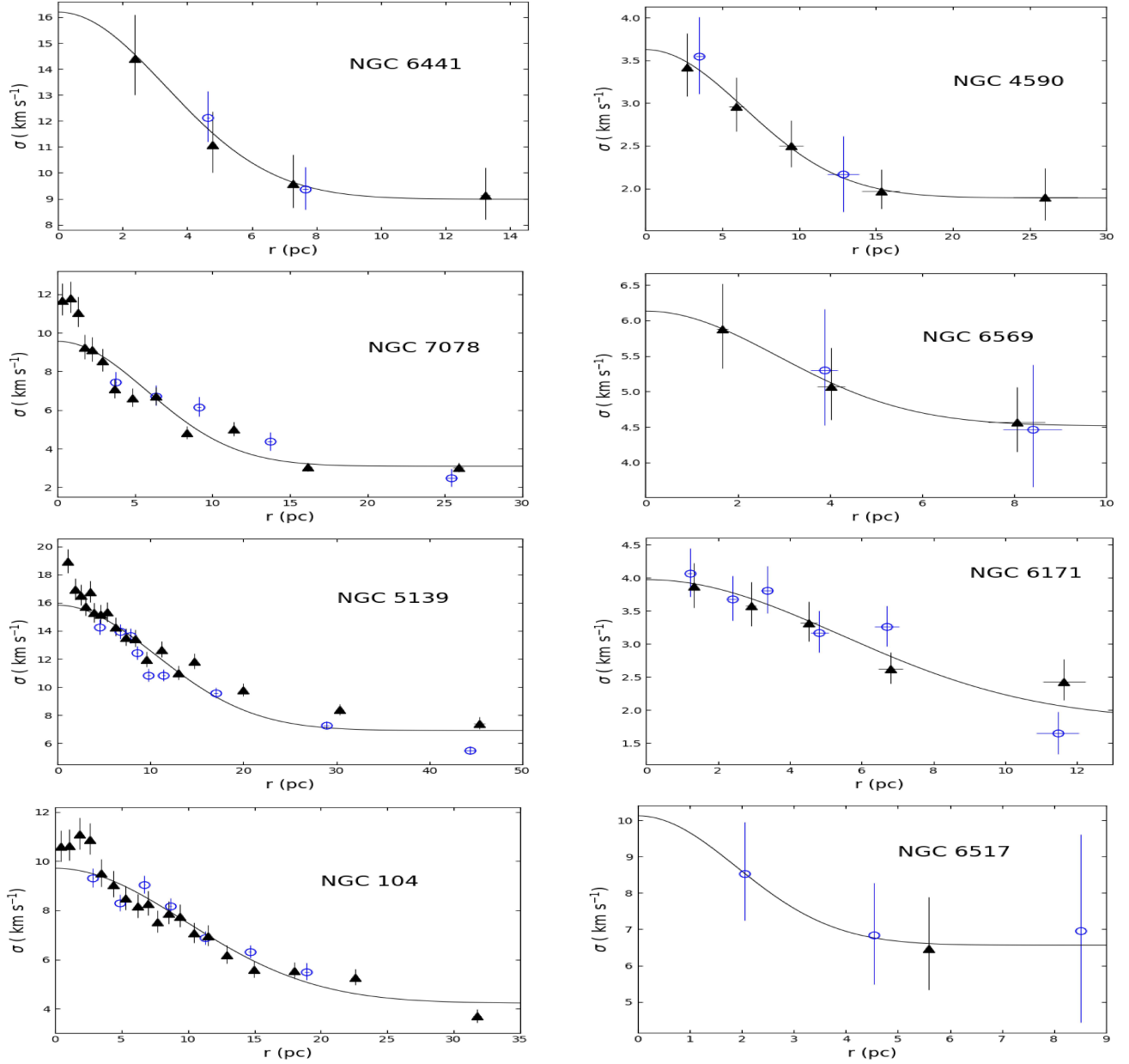


Figure 1. The figure shows eight examples of the velocity dispersion profile fits to equation (1) performed, covering the range of morphologies of profiles found. The solid triangles show ESO Keck radial dispersion velocity measurements, and the circles give Gaia DR2 data, with no systematic offset being present between the two, from the Baumgardt et al. (2019) catalogue. The good representation of the empirical profiles afforded by equation (1) which is evident here, applies also to the full sample, which appears in the figures of the online material.

and as central values, the means of the central values of the three models provided. Notice that we do not use any dynamical models to determine total masses, so that the final parameters obtained are purely empirical and fully independent of any assumptions on the structure of gravity at any scale. The total magnitudes in the V band we take from the most recent update of the Harris catalogue, Harris (1996), 2010 edition, and distances consistently from Baumgardt et al. (2019) to infer the total stellar masses for the GCs in our final sample, given in the last column of table 1.

3 A TULLY-FISHER RELATION FOR GCS

Having obtained the best currently available estimates for σ_∞ and M for the GCs in our sample, in Figure (2) we give our final result for the 40 GCs treated, with corresponding error bars. The solid line in this figure shows a linear best fit of $\sigma_\infty(\text{km s}^{-1}) = 0.084^{+0.075}_{-0.040}(M/M_\odot)^{0.3 \pm 0.051}$. This is consistent with the expected scaling of $\sigma_\infty(\text{km s}^{-1}) = 0.2(M/M_\odot)^{0.25}$ for isolated pressure supported systems in MOND. Thus, the trend observed in Figure (2) represents an equivalent empirical relation to the well known baryonic Tully-Fisher for disk galaxies, both consistent with a fixed underlying trend, once the difference between full centrifugal support and close to isothermal pressure support is taken

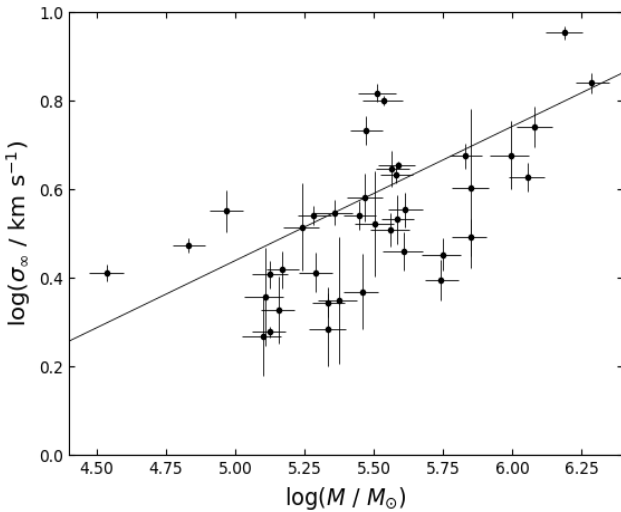


Figure 2. The figure shows asymptotic large radii projected velocity dispersion values, σ_∞ , and corresponding stellar population total mass estimates, M , for 40 Galactic globular clusters with high quality kinematic profile observations, on a log-arithmetic plot. The line gives a best linear fit to the data, yielding $\sigma_\infty(kms^{-1}) = 0.084^{+0.075}_{-0.040}(M/M_\odot)^{0.3 \pm 0.051}$, which is consistent with deep MOND expectations of $\sigma_\infty(kms^{-1}) = 0.2(M/M_\odot)^{0.25}$.

into account. However, one difference between our result and the galactic Tully-Fisher relation is evident, the presence of a significant intrinsic scatter in the data, well above what appears in spiral galaxies.

A number of caveats must be mentioned, firstly, it is now known that many Galactic globular clusters, if not all, show in the details some evidence for the presence of multiple stellar populations (see Cordoni et al. 2019 and Pasquato & Milone 2019 and references therein for two recent examples), so that the single stellar population assumption taken in McLaughlin & van der Marel (2005) to derive the mass to light ratios used, is only a first order approximation. Thus, the confidence intervals on the mass estimates we use here are probably an underestimation. The same happens when considering the possibility of Salpeter stellar mass functions, which do not alter the resulting power law fit, but do shift the data to the right by a small factor. Accounting for the two above effects, to some varying degree in the different GCs, might also reduce the effective scatter observed and make the distribution more compatible with a single power law.

Also, the analogy with centrifugally supported disks breaks down when considering that in that case, the kinematically observed quantity offers a very direct determination of the dynamics, beyond minor details introduced by effects such as asymmetric drift and gas pressure, when considering radio observations. In the case of globular clusters however, stellar orbits are much closer to isothermal distributions, where the stars observed at a given radius actually sample during their orbits a very large range of radii, and hence of radial forces. The details of the above will be strongly dependent on the particular features of each cluster, such as orbital anisotropy parameters (even radial variations in this quantity) and the degree of central concentration in the present day density profiles. Thus, it is perfectly possible that in Figure (2) we are seeing the superposition of a series

of 'Tully-Fisher' relations, the disentangling of which will await more detailed data than the ones presently available.

It is however encouraging, that inspite of the presence of the complications mentioned above, a very clear trend appears, and it is extremely interesting that this trend should be consistent, to within internal confidence intervals, with MOND expectations for isolated systems.

This result is a challenge for some of the Newtonian explanations for the observed outer flattening of the velocity dispersion profile of globular clusters, such as the appearance of chaotic dynamics investigated by Claydon et al. (2017), or the influence of tidal fields explored in Lane et al. (2012), both of which depend on the mass of the cluster such that the extra dynamical heating effects considered diminish in importance as the mass of the cluster in question increases. Thus, being problematic the understanding of a clear positive trend as the one shown in Figure (2), consistent with a Tully-Fisher scaling.

From the point of view of MOND as such, the situation is not much different, as most of the clusters treated lie at relatively small galactocentric distances, and would hence be expected to lie within the region where the external field effect dominates, and no significant departure from Newtonian dynamics would be expected (e.g. Famaey & McGaugh 2012). From this latter point of view, our results would point towards a modified MONDian gravity theory where the external field effect is much less relevant (if at all) than in the case of MOND, e.g. Milgrom (2011).

4 CONCLUSIONS

We have taken a large homogeneous sample of published velocity dispersion profiles for 40 Galactic globular clusters, to study the first order characteristics of the kinematics of these systems in their outer low acceleration regions.

We find that a simple central Gaussian region and a flat asymptote, σ_∞ , are sufficient to very accurately model all the observed velocity dispersion profiles treated.

Estimating masses from stellar population models not including any dynamical assumptions, then allows to investigate the empirical relation existing between σ_∞ and M . While no *a priori* relation between these two parameters was assumed or forced, the results show a very clear signal consistent with the isothermal pressure supported equivalent of the baryonic Tully-Fisher relation in disk galaxies, of $\sigma_\infty(kms^{-1}) = 0.2(M/M_\odot)^{0.25}$.

This result becomes a further constraint towards understanding the formation and evolution of globular clusters, under either a Newtonian framework, or within any alternative theory of gravity.

ACKNOWLEDGEMENTS

Xavier Hernandez acknowledges financial assistance from UNAM DGAPA grant IN104517 and CONACYT.

REFERENCES

Baumgardt H., Hilker M., 2018, MNRAS, 478, 1520

Table 1. Parameters for the globular clusters treated.

GC	$\sigma_1(km/s)$	$\sigma_\infty(km/s)$	R_σ (pc)	$\log(M/M_\odot)$
NGC 104	5.49±0.35	4.22±0.33	13.87±1.12	6.06 ^{+0.06} _{-0.07}
NGC 362	3.96±0.28	2.87±0.30	10.68±1.12	5.61 ^{+0.07} _{-0.08}
NGC 1261	2.03±0.38	1.92±0.40	15.41±3.51	5.33 ^{+0.07} _{-0.07}
NGC 1851	3.06±0.44	3.22±0.29	10.63±1.95	5.56 ^{+0.07} _{-0.07}
NGC 1904	1.88±0.19	2.21±0.17	12.54±1.74	5.33 ^{+0.06} _{-0.06}
NGC 2808	5.32±0.83	4.75±0.93	14.91±3.12	5.99 ^{+0.07} _{-0.08}
NGC 3201	1.31±0.26	2.62±0.27	6.93±1.70	5.17 ^{+0.06} _{-0.06}
NGC 4372	1.96±0.24	2.58±0.27	9.72±1.63	5.29 ^{+0.06} _{-0.06}
NGC 4590	1.74±0.09	1.89±0.06	9.09±0.64	5.12 ^{+0.06} _{-0.06}
NGC 4833	1.25±0.55	3.48±0.27	3.98±1.97	5.45 ^{+0.06} _{-0.06}
NGC 5139	8.92±0.58	6.90±0.38	14.87±1.36	6.29 ^{+0.06} _{-0.06}
NGC 5272	4.26±0.40	2.48±0.28	12.78±1.69	5.74 ^{+0.06} _{-0.06}
NGC 5904	3.75±0.23	2.83±0.24	13.94±1.34	5.75 ^{+0.07} _{-0.07}
NGC 5927	2.35±0.95	3.32±1.04	12.79±5.51	5.50 ^{+0.07} _{-0.07}
NGC 5986	3.49±1.11	4.43±0.44	4.64±1.51	5.56 ^{+0.06} _{-0.06}
NGC 6093	4.02±0.83	5.39±0.42	2.58±0.64	5.47 ^{+0.06} _{-0.06}
NGC 6121	2.22±0.61	2.27±0.65	5.16±1.29	5.11 ^{+0.07} _{-0.08}
NGC 6171	2.13±0.38	1.84±0.42	7.67±1.83	5.10 ^{+0.06} _{-0.08}
NGC 6205	3.38±0.34	3.57±0.34	12.14±1.71	5.61 ^{+0.06} _{-0.06}
NGC 6218	1.61±0.23	2.55±0.19	4.32±0.86	5.12 ^{+0.07} _{-0.06}
NGC 6273	7.09±0.42	4.73±0.32	6.82±0.56	5.83 ^{+0.06} _{-0.06}
NGC 6304	2.15±0.67	3.26±0.84	3.25±1.56	5.24 ^{+0.06} _{-0.07}
NGC 6341	3.85±0.65	2.33±0.50	12.63±2.44	5.46 ^{+0.06} _{-0.07}
NGC 6388	6.02±0.54	5.50±0.62	11.34±1.74	6.08 ^{+0.06} _{-0.07}
NGC 6397	1.62±0.11	2.96±0.12	3.94±0.40	4.83 ^{+0.06} _{-0.06}
NGC 6402	5.34±1.69	3.99±2.04	11.15±4.79	5.85 ^{+0.07} _{-0.07}
NGC 6441	7.21±0.87	8.98±0.31	4.69±0.49	6.19 ^{+0.06} _{-0.07}
NGC 6517	3.56±1.69	6.56±0.32	2.68±1.29	5.51 ^{+0.07} _{-0.07}
NGC 6541	2.49±0.42	3.39±0.47	8.83±1.80	5.59 ^{+0.06} _{-0.06}
NGC 6544	2.61±0.38	3.55±0.41	2.65±0.40	4.97 ^{+0.06} _{-0.06}
NGC 6553	2.48±1.20	6.30±0.16	1.67±0.51	5.54 ^{+0.07} _{-0.08}
NGC 6569	1.62±0.14	4.52±0.07	4.07±0.40	5.59 ^{+0.06} _{-0.07}
NGC 6624	2.75±0.50	3.52±0.24	1.76±0.39	5.36 ^{+0.07} _{-0.07}
NGC 6626	4.74±0.43	3.81±0.49	5.70±0.72	5.47 ^{+0.07} _{-0.06}
NGC 6656	3.62±0.18	4.29±0.19	6.48±0.50	5.58 ^{+0.06} _{-0.06}
NGC 6723	2.89±0.81	2.23±0.87	8.43±2.85	5.37 ^{+0.07} _{-0.08}
NGC 6752	2.99±0.27	3.47±0.17	5.55±0.58	5.28 ^{+0.06} _{-0.06}
NGC 6838	1.48±0.87	2.57±0.11	0.89±0.35	4.54 ^{+0.06} _{-0.07}
NGC 7078	6.47±0.56	3.09±0.31	8.15±0.94	5.85 ^{+0.06} _{-0.07}
NGC 7099	2.10±0.44	2.12±0.40	8.35±2.80	5.15 ^{+0.06} _{-0.06}

After the globular cluster identification column, the following three entries give the parameters of the fits to equation(1) for the observed projected velocity dispersion profiles of Baumgard et al. (2019) and their confidence intervals. The last column gives total stellar mass estimates from the stellar population modelling of McLaughlin & van der Marel (2005).

Baumgardt H., Hilker M., Sollima A., Bellini A., 2019, MNRAS, 482, 5138
Claydon I., Gieles M., Zocchi A., 2017, MNRAS, 466, 3937
Cordonì, G., Milone, A. P., Mastrobuono-Battisti, A., et al. 2019, arXiv:1905.09908
Durazo R., Hernandez X., Cervantes Sodi B., Sanchez S. F., 2017, ApJ, 837, 179
Durazo R., Hernandez X., Cervantes Sodi B., Sanchez S. F., 2018, ApJ, 863, 107
Famaey B., McGaugh S.S., 2012, LRR, 15, 10
Harris, W.E. 1996, AJ, 112, 1487
Hernandez X., Jimenez M. A., 2012, ApJ, 750, 9
Hernandez X., Jimenez M. A., Allen C., 2013, MNRAS, 428, 3196
Hernandez X., Cortes R. A. M., Scarpa R., 2017, MNRAS, 464, 2930
Kennedy G. F., 2014, MNRAS, 445, 4446
Lane R. R., Kiss L. L., Lewis G. F., Ibata R. A., Siebert A., Bedding T. R., Szkely P., 2009, MNRAS, 400, 917
Lane R. R., Kiss L. L., Lewis G. F., Ibata R. A., Siebert A., Bedding T. R., Szkely P., 2010, MNRAS, 401, 2521
Lane R. R., Kiss L. L., Lewis G. F., Ibata R. A., Siebert A., Bedding T. R., Szekely P., Szabo G. M., 2011, A&A, 530, A31
Lane R. R., Kupper A. H. W., Heggie D. C., 2012, MNRAS, 423, 2845
Lelli F., McGaugh S. S., Schombert J. M., Pawlowski M. S., 2017, ApJ, 836, 152
Pasquato M., Milone A., 2019, arXiv:1906.04983
McGaugh, S., & Wolf, J. 2010, ApJ, 722, 248
McLaughlin D. E., van der Marel R. P., 2005, ApJS, 161, 304
Milgrom M., 1983, ApJ, 270, 365
Milgrom, M. 2011, AcPPB, 42, 2175
Scarpa R., Marconi G., Gilmozzi R., 2003, A&A, 405, L15
Scarpa R., Marconi G., Gilmozzi R., Carraro G., 2007, A&A, 462, L9
Sollima A. et al., 2016, MNRAS, 462, 1937

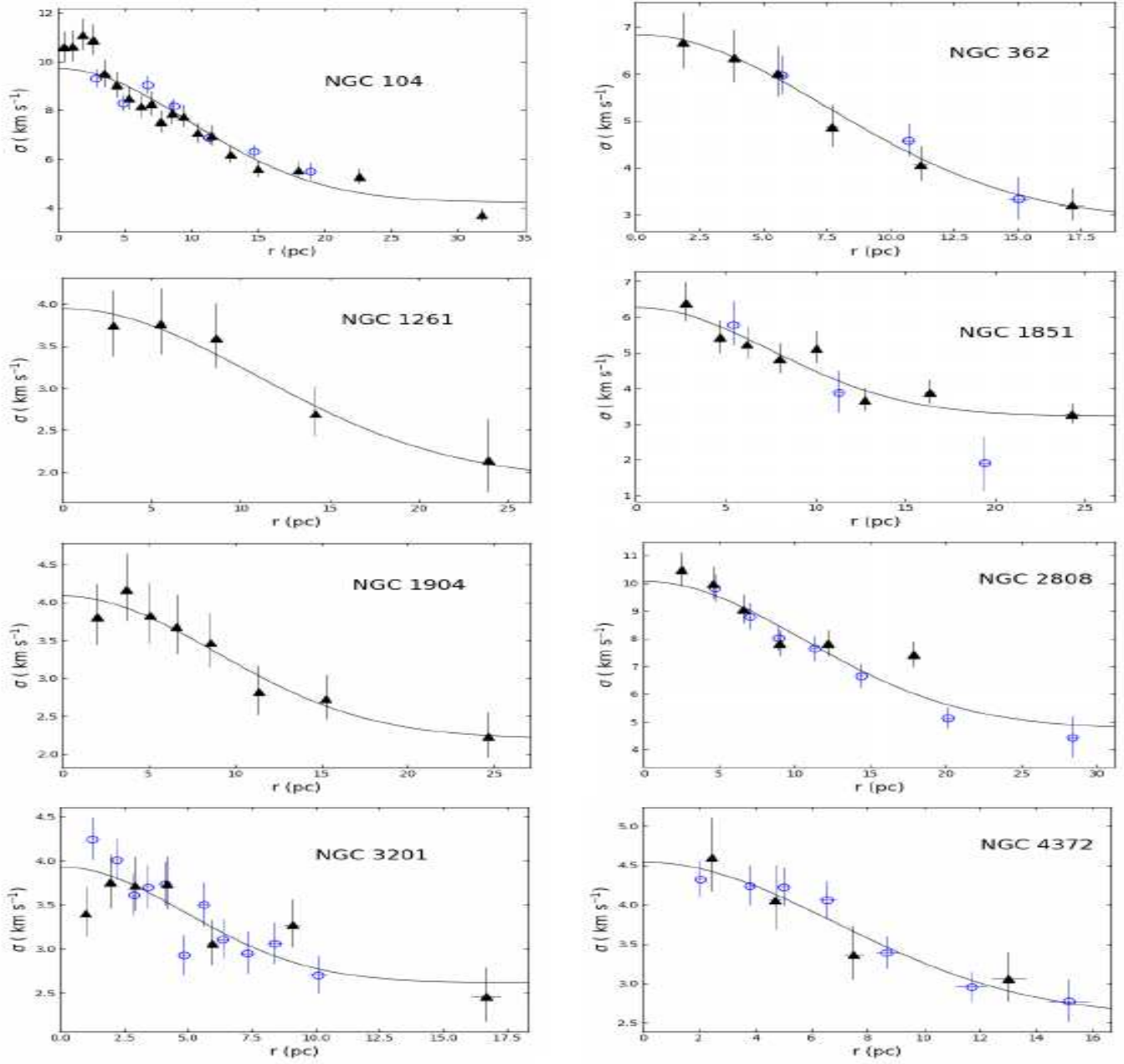


Figure 3. The figure shows the first eight velocity dispersion profile fits to equation (1). The solid triangles show ESO Keck radial dispersion velocity measurements, and the circles give Gaia DR2 data, with no systematic offset being present between the two, from the Baumgardt et al. (2019) catalogue. That a good representation of the empirical profiles is afforded by equation (1) is evident.

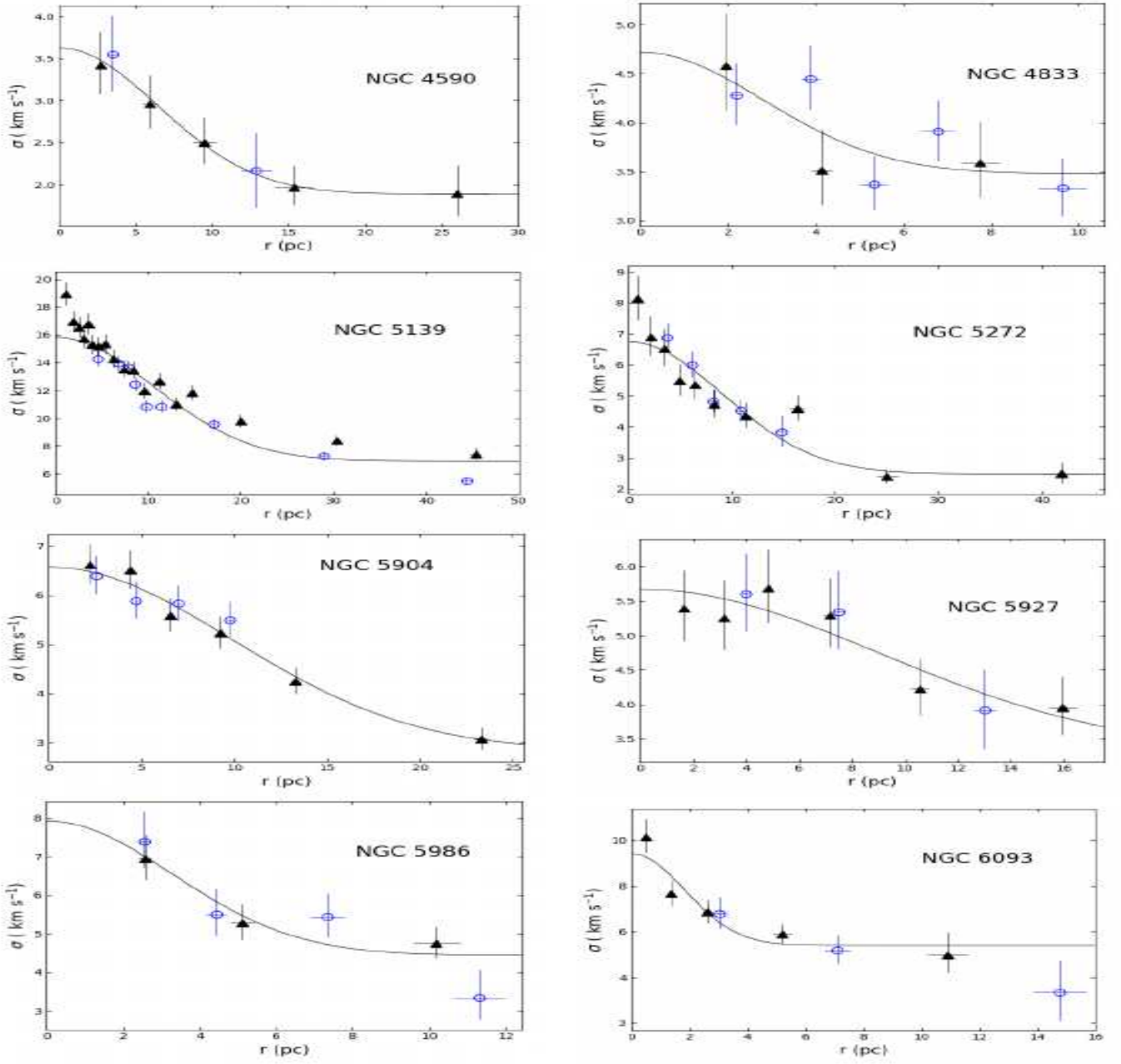


Figure 4. The figure shows the first eight velocity dispersion profile fits to equation (1). The solid triangles show ESO Keck radial dispersion velocity measurements, and the circles give Gaia DR2 data, with no systematic offset being present between the two, from the Baumgardt et al. (2019) catalogue. That a good representation of the empirical profiles is afforded by equation (1) is evident.

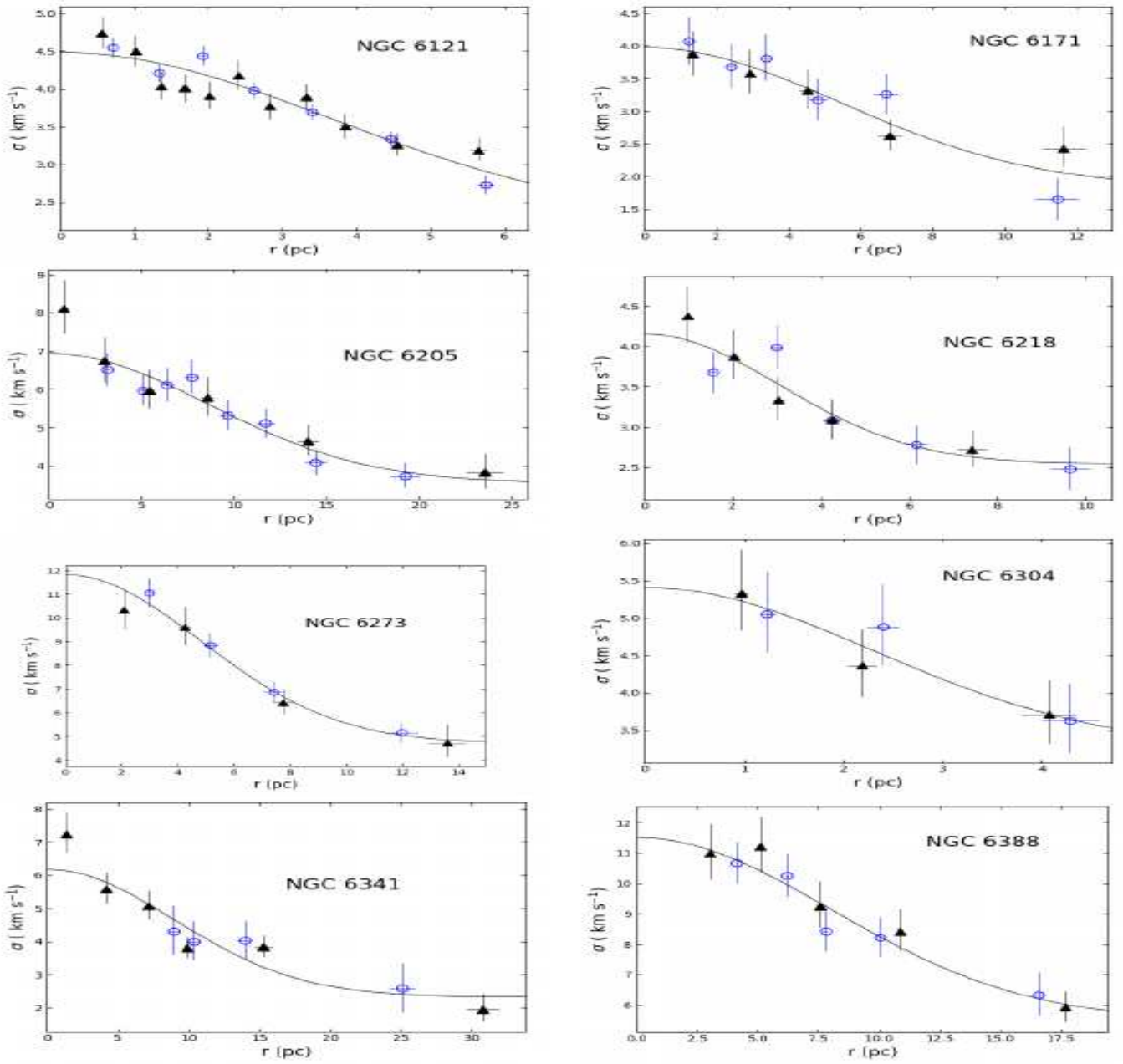


Figure 5. The figure shows the first eight velocity dispersion profile fits to equation (1). The solid triangles show ESO Keck radial dispersion velocity measurements, and the circles give Gaia DR2 data, with no systematic offset being present between the two, from the Baumgardt et al. (2019) catalogue. That a good representation of the empirical profiles is afforded by equation (1) is evident.

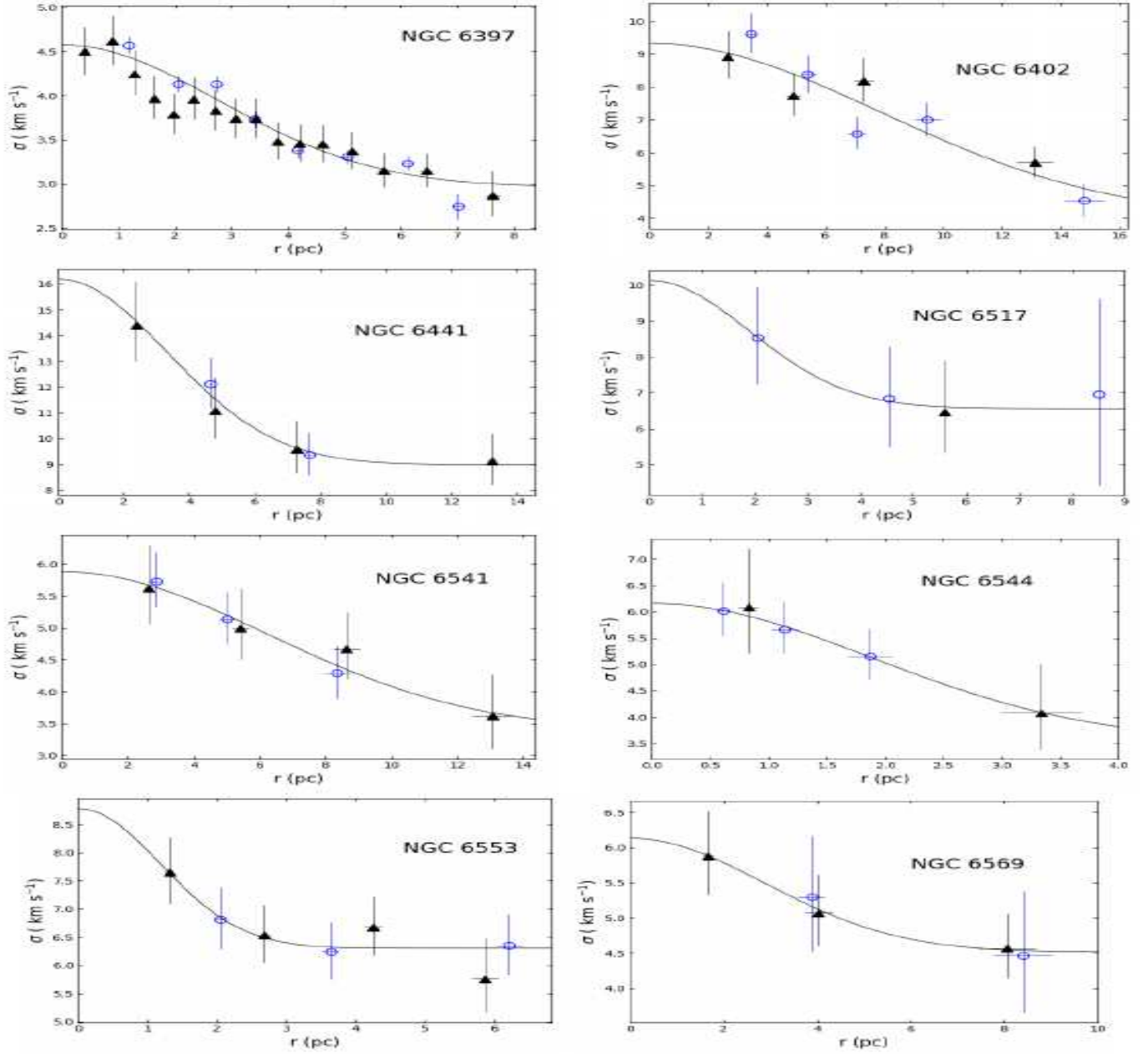


Figure 6. The figure shows the first eight velocity dispersion profile fits to equation (1). The solid triangles show ESO Keck radial dispersion velocity measurements, and the circles give Gaia DR2 data, with no systematic offset being present between the two, from the Baumgardt et al. (2019) catalogue. That a good representation of the empirical profiles is afforded by equation (1) is evident.

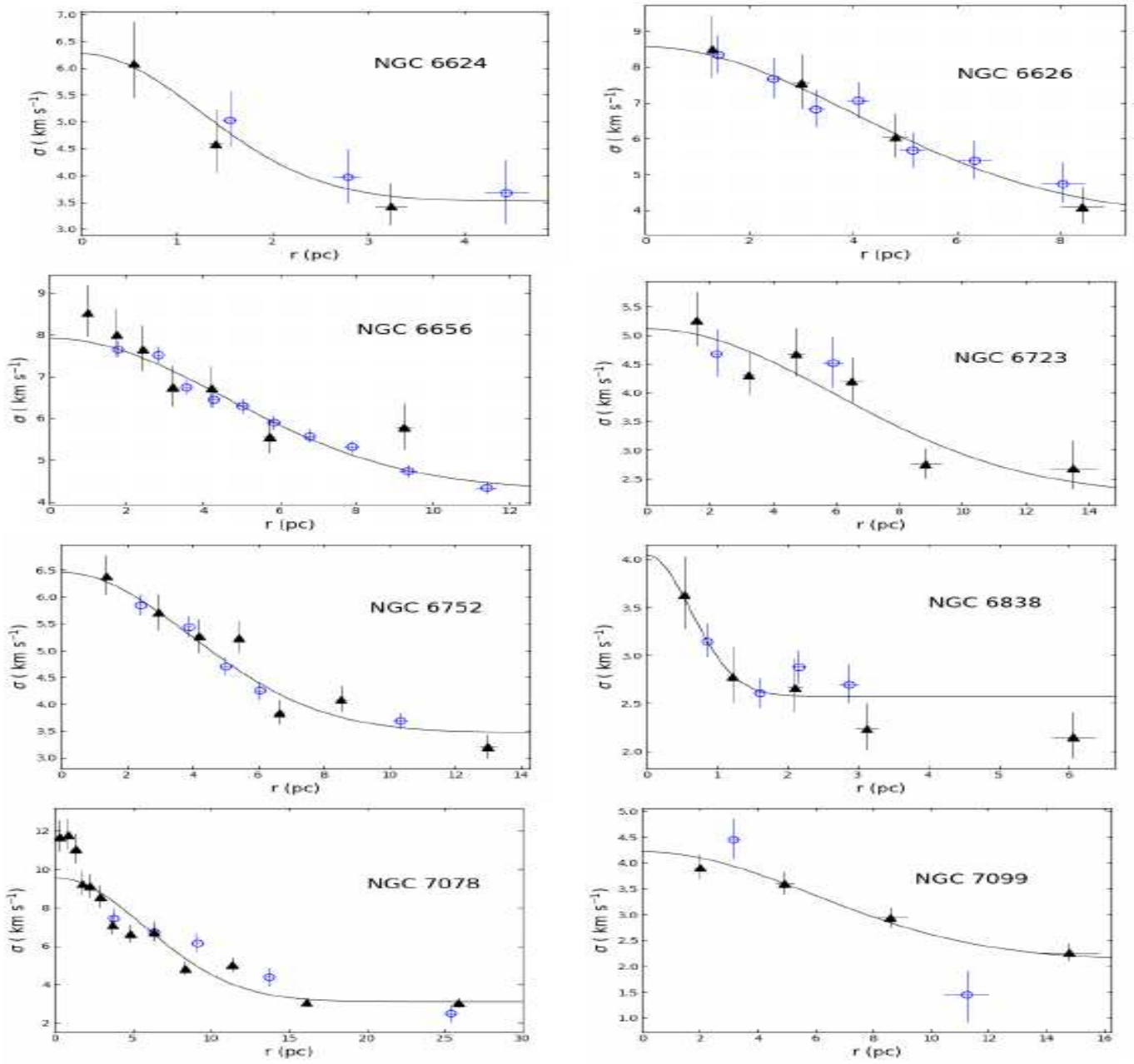


Figure 7. The figure shows the first eight velocity dispersion profile fits to equation (1). The solid triangles show ESO Keck radial dispersion velocity measurements, and the circles give Gaia DR2 data, with no systematic offset being present between the two, from the Baumgardt et al. (2019) catalogue. That a good representation of the empirical profiles is afforded by equation (1) is evident.